

Interlaminar Toughening of GFRP—Part II: Characterization and Numerical Simulation of Curing Kinetics

Dakai Bian¹

Department of Mechanical Engineering,
Columbia University,
New York, NY 10027
e-mail: db2875@columbia.edu

Bradley R. Beeksm

Department of Mechanical Engineering,
Columbia University,
New York, NY 10027

D. J. Shim

GE Global Research,
Niskayuna, NY 12309

Marshall Jones

GE Global Research,
Niskayuna, NY 12309

Y. Lawrence Yao

Department of Mechanical Engineering,
Columbia University,
New York, NY 10027

Various methods of toughening the bonding between the interleaf and laminate glass fiber reinforced polymer (GFRP) have been developed due to the increasing applications in industries. A polystyrene (PS) additive modified epoxy is used to improve the diffusion and precipitation region between polysulfone (PSU) interleaf and epoxy due to its influence on the curing kinetics without changing glass transition temperature and viscosity of the curing epoxy. The temperature-dependent diffusivities of epoxy, amine hardener, and PSU are determined by using attenuated total reflection–Fourier transfer infrared spectroscopy (ATR–FTIR) through monitoring the changing absorbance of their characteristic peaks. Effects of PS additive on diffusivity in the epoxy system are investigated by comparing the diffusivity between nonmodified and PS modified epoxy. The consumption rate of the epoxide group in the curing epoxy reveals the curing reaction rate, and the influence of PS additive on the curing kinetics is also studied by determining the degree of curing with time. A diffusivity model coupled with curing kinetics is applied to simulate the diffusion and precipitation process between PSU and curing epoxy. The effect of geometry factor is considered to simulate the diffusion and precipitation process with and without the existence of fibers. The simulation results show the diffusion and precipitation depths which match those observed in the experiments. [DOI: 10.1115/1.4036127]

Keywords: curing kinetics, diffusivity model, diffusion and precipitation, ATR–FTIR

Introduction

The methods to toughen the fiber reinforced polymer have been studied in the past decades. Thermoplastic (TP) materials have been considered as potential materials because the ductile behavior of TP can absorb more energy when the crack propagates. Many industries used high-performance TP like polycarbonate, polymethylmethacrylate, polyetherimide, polysulfone, and polyethersulfone, which have been studied as a modifier to the epoxy [1–4]. Results indicate that even though TP has high strength and toughness, the adhesion failure can still occur if the TP cannot bond well with the thermoset (TS) epoxy.

Thus, choosing a compatible TP to the epoxy is vital to improve the bonding quality because a semi-interpenetration network (semi-IPN) region can be generated between the TP and the epoxy [5,6]. The long chain of compatible TPs can relax and increase the free space inside, which let the low molar mass curing epoxy diffuse into these spaces. On the other hand, the relaxed TPs disentangle and flow into the curing epoxy out from the solid TPs' region. Finally, the long-chain TPs entangle with the crosslinked cured epoxy, which is semi-IPN. This network is the key to improve better bonding between TPs and TSs and avoid the adhesion failure.

For polymers, diffusion is dependent on many factors. Compatible polymer–polymer systems need to be chosen based on the solubility theory: the closer the solubility parameters of the two polymers are to each other, the more likely they will have diffusion [7]. Typically, TP is of high molecular weight and high viscosity. Thus, TP often cannot diffuse easily within the acceptable time regime of the bonding operations like the curing process of epoxy. Improved adhesion due to diffusion and precipitation of

molecules is hard to realize except by significantly increasing the mobility of the molecular chains of the two polymers by applying heat or solvent [8–10]. Diffusing molecules would also need to find their way around impermeable particles such as fibers in the matrix, increasing path lengths, and reducing mass transport rates [11].

The mechanical behavior of PS modified epoxy and the morphology of improved diffusion and precipitation region was studied in Part I of this paper [12]. The results indicated that deep diffusion and precipitation were critical to the high toughness. Thus, in this study, diffusivity of polymers and curing kinetics of the system were characterized by using ATR–FTIR technique. The changing peaks of curing epoxy system were monitored to quantify the diffusivity of species at different curing temperatures. Numerical methods were used to predict and optimize the experiment results with and without the existence of the glass fiber reinforced polymer. The dependence of diffusivity and curing kinetics as well as diffusion and precipitation mechanism at the interface between TP and TS were investigated and discussed.

Background

Chemical Reactions of the Curing Process. The cure of epoxy resin with amine crosslinking agents proceeds primarily through the addition reaction between the epoxide ring and amine hydrogen, as shown in Fig. 1. Figure 1(a) shows that during the reaction with primary amine, the epoxide ring opens, bond formation occurs between the terminal carbon of the epoxy and amine nitrogen. In Fig. 1(b), reaction of the resultant secondary amine with another epoxy molecule results in a tertiary amine which acts as a branch point. The repetitions of this reaction scheme lead to the construction of a highly branched, high molecular weight network structure. Since the cure reaction produces hydroxyl groups, the reaction should be autocatalytic, which means the hydrogen in

¹Corresponding author.

Manuscript received November 21, 2016; final manuscript received February 14, 2017; published online March 24, 2017. Assoc. Editor: Donggang Yao.

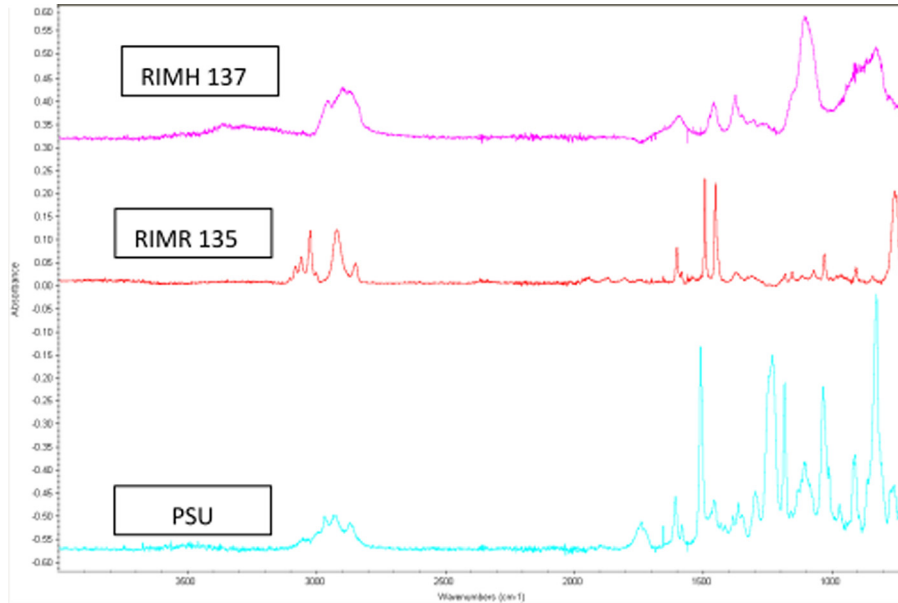


Fig. 2 ATR-FTIR spectra of RIMH 137 curing agent, RIMR 135 resin, and PSU. Peaks monitored during diffusion experiments: 915 cm^{-1} (epoxide deformation) and 1036 cm^{-1} (aromatic deformation) in RIMR 135; 2916 cm^{-1} (C-H stretching of diamine) for RIMH 137; and 1151 cm^{-1} (S=O stretching) for PSU.

chloride solution with an approximately 5% weight concentration. One coat at 500 rpm for 10 s by using spin coating consistently produced $5\text{ }\mu\text{m}$ film, of which the thickness is suitable so that the results are not sensitive to variations in the penetration depth of the infrared [14]. RIMR 135 epoxy resin (modified and nonmodified) and RIMH 137 hardener were dropped on the thin film at different temperatures separately. Since FTIR provided information through the change in peak height or peak area with time and the peaks presented specific chemical groups in the molecules, some characteristic peaks such as 915 cm^{-1} (epoxide ring deformation), 1151 cm^{-1} (S=O bond), and 2915 cm^{-1} (C-H stretching in the hardener spectra) were monitored. Spectra were taken every few minutes early in the diffusion and several times an hour at longer time. For the second objective, there was no film on the IR crystal, epoxy resin (modified and nonmodified) and hardener were pre-mixed and dropped directly on the surface of the IR crystal under different temperatures. Peaks that represented epoxide ring were monitored at various times.

Numerical Simulation

Diffusivity of Species in the Epoxy System. By assuming Fickian diffusion kinetics, ATR-FTIR technique was used to study the individual diffusion of epoxy and amine monomers into PSU and PSU into the epoxy or hardener bath. The model geometry is showed in Fig. 3. The general Fickian and Fick's second law is

$$\frac{\partial C_p}{\partial t} = D_p \frac{\partial^2 C_p}{\partial x^2} \quad (3)$$

where p represents penetrant, either epoxy or amine. Assuming the concentration of amine or epoxy in the film is zero at the beginning, the solution to the diffusion equation is [15]

$$\frac{A(t) - A_\infty}{A_0 - A_\infty} = \frac{\sum_{n=0}^{\infty} F_n \exp\left(-\left(\frac{(2n+1)\pi}{2l}\right)^2 Dt\right)}{\sum_{n=0}^{\infty} F_n} \quad (4)$$

$$F_n = \left[\frac{(-1)^n l}{2n+1 d_p} + \frac{\pi}{4} \exp\left(-2\frac{l}{d_p}\right) \right] * \left\{ [(2n+1)\pi]^2 + 16\left(\frac{l}{d_p}\right)^2 \right\}^{-1} \quad (5)$$

where A is the absorbance, D is the diffusivity of the penetrant at current temperature, l is the film thickness, and d_p is the penetration depth of the infrared at specific wavelength. In this expression, the diffusivity is the only fitting parameter and is of the Arrhenius diffusivity relationship with temperature

$$D_p(T) = C \exp\left(-\frac{D}{RT}\right) \quad (6)$$

where p represents the penetrant, and C and D are constant coefficients.

Curing Kinetics of the Epoxy System. The curing kinetics is assumed to be proportional to the rate of heat generation, which

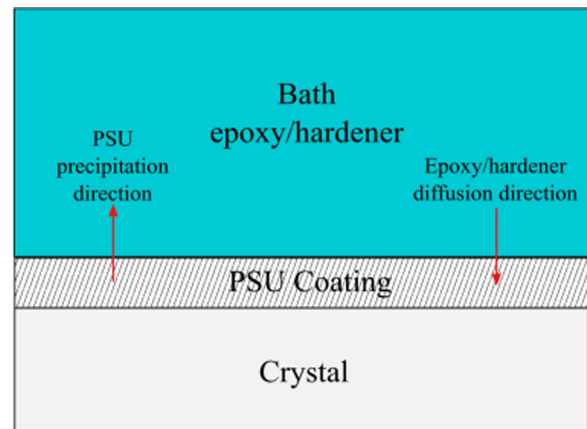


Fig. 3 FTIR experiment setup for determination of diffusivity and curing kinetics

can be defined by two separable parameters: K and α [16]. The simplest model corresponds to an n th-order kinetic expression

$$\frac{d\alpha}{dt} = K(1 - \alpha)^n \quad (7)$$

where α is the degree of cure in the system

$$\alpha = 1 - \frac{c_e}{c_{e0}} = 1 - \frac{c_a}{c_{a0}} \quad (8)$$

where c_e and c_a are the epoxide and amine hydrogen concentrations at any time, 0 indicates the initial condition, n is the reaction order, and K is the rate constant given by an Arrhenius temperature dependence.

Assumed that the secondary amine group formed in the reaction shows the same degree of reactivity toward epoxy groups as the primary amine groups, the total rate of consumption of epoxides

$$\frac{d\alpha}{dt} = (k_1 + k_2\alpha)(1 - \alpha)^2 \quad (9)$$

$$k_1 = A_1 \exp\left(-\frac{E_1}{RT}\right) \quad (10)$$

$$k_2 = A_2 \exp\left(-\frac{E_2}{RT}\right) \quad (11)$$

where A_1, A_2 are pre-exponential constants; E_1, E_2 are the activation energies; R is the ideal gas constant; and T is temperature. These equations represent the intrinsic kinetics, and they only depend on the chemical nature of the reacting species.

The glass transition temperature reflects the amount of free volume in the curing TS available for diffusion or precipitation. As the glass transition temperature increases, the mobility of the molecules decreases and the system becomes rigid. The DiBenedetto model is used to provide a reliable relation between the glass transition temperature of the curing epoxy and the degree of curing [17]. By relating DiBenedetto equation and free volume theory [18], the diffusivity expression becomes

$$D = D_p \exp\left(B\left(1 - \frac{1}{0.025 + \beta(T - T_g(\alpha(t)))}\right)\right) \quad (12)$$

for most cases, B is 0.9–1.2.

Thus, the general governing equation for epoxy and curing agent transport in the TP is [18,19]

$$\frac{\partial C_p(\alpha)}{\partial t} = \frac{\partial}{\partial x} \left(\frac{\partial C_p(\alpha)}{\partial x} \right) D_p(\alpha) - R_r(\alpha) \quad (13)$$

where C_p is the concentration of the species, and $R_r(\alpha)$ represents the reaction rate, which is Eq. (9).

Since the TP does not have the curing reaction, the governing equation for TP transport in the epoxy-rich region is

$$\frac{\partial C_p(\alpha)}{\partial t} = \frac{\partial}{\partial x} \left(\frac{\partial C_p(\alpha)}{\partial x} \right) D_p(\alpha) \quad (14)$$

Results and Discussion

ATR-FTIR technology was used to determine the diffusivity between the epoxy system and the PSU experimentally. Since the entire process was the superposition of the diffusion and precipitation process, and the curing process, it was important to simplify the complexity of the problem. It was assumed that the diffusivity

was dependent on temperature, degree of curing, and free space in the diffusion direction, which meant the entire process could be experimentally determined from three aspects: single component diffusivity (D_p in Eq. (12)), curing kinetics (α in Eq. (9)), and structure factor.

Diffusivity Determination of the Epoxy System. By monitoring the absorbance change of the FTIR spectra, the concentration of species was determined at the specific time. As can be seen from Fig. 4, it showed the FTIR spectra of 1151 cm^{-1} peak ($S=O$ stretching in the PSU) decreased with the increasing time, which indicated that from 1 min to 230 min, in the infrared penetration region, diffusion and precipitation process was happening that reduced the concentration of the PSU. The PSU film coated on the crystal shown in Fig. 3 was initially thicker than the penetration depth of infrared lights. As the diffusion and precipitation proceeded, epoxy/hardener began to penetrate into the PSU film, and PSU molecules began to flow into the bath. Thus, the reduced concentration of PSU and the increased concentration of epoxy/hardener in the infrared penetration region led to the reduction of PSU peak intensity and the increment of penetrant peak intensity. Based on this principle, the different characteristic peaks were monitored during the experiments for diffusivity determination or curing kinetics.

The experiment setup for determination of the diffusivity was that a thin PSU film was first spin-coated on the infrared crystal element, and 1 ml of epoxy or hardener was dropped on the film surface at various temperatures. Figure 5 shows the experimental results of PSU into epoxy at four processing temperatures. The dots represented the normalized absorbance of the 1151 cm^{-1} peaks at the moment of measurement. The 1151 cm^{-1} peak was for the $S=O$ stretching in the PSU. From the figure, the peak reduced rapidly in the beginning at high processing temperatures but reduced slowly at low temperatures. The reason for the concentration drop was that the absorbance of the peak represented the concentration of the species with this specific chemical bond. When the hardener started to contact with the PSU surface, it swelled the long-chain TP. The relaxation of the long-chain structure produced more free space in between, where the epoxy began to diffuse into and fill the free space and PSU began to flow into the epoxy bath in the opposite direction, which led to the reduction of the concentration of the PSU. After a period of time, the concentration of two species approached to steady-state, which led to the level off of the data points. The processing temperature

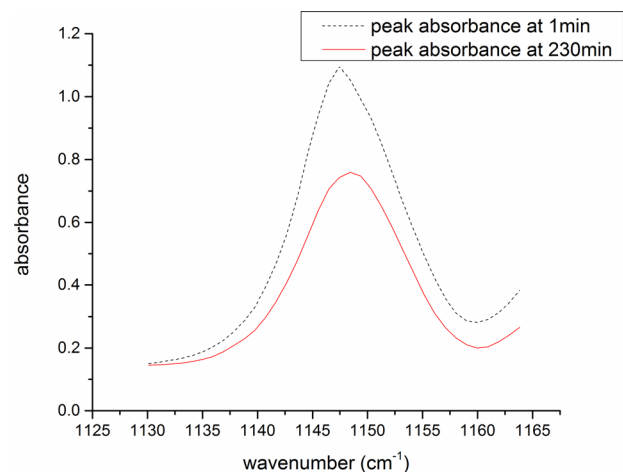


Fig. 4 Typical FTIR spectra of 1151 cm^{-1} peak ($S=O$ stretching) decreased with the increasing time observed in the experiment. The diffusivity and reaction rate are both obtained by monitoring the absorbance changes of characteristic peaks with time.

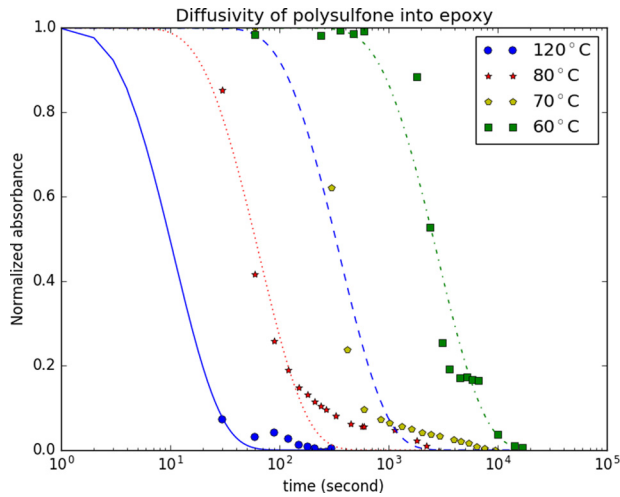


Fig. 5 Diffusivity determination of PSU into epoxy from 60 °C to 120 °C. Normalized absorbance data were obtained from ATR–FTIR experiments. Least square fitting curves were based on Eq. (4) for each condition.

significantly influenced the diffusivity. At 120 °C, the normalized absorbance of PSU dropped to less than 0.1 in 30 s. However at 60 °C, it took almost 10,000 s to drop to 0.1. By using the relationship between absorbance and diffusivity shown in Eq. (4), least square fitting curves were plotted in Fig. 5 for each condition. From 60 °C to 120 °C, the diffusivity of PSU into epoxy at each condition was 1.31×10^{-11} , 1.03×10^{-10} , 5.611×10^{-10} , and 1.01×10^{-7} m²/s. The corresponding experimental results of epoxy into PSU are shown in Fig. 6. From 60 °C to 120 °C, the diffusivity of epoxy into PSU at each condition was 1.71×10^{-11} , 2.05×10^{-10} , 9.991×10^{-10} , and 2.23×10^{-7} m²/s. The results were reasonable, since the diffusivity was highly dependent on the processing temperatures and the difference between 60 °C and 120 °C was 4 orders of magnitude. Based on the diffusivity of epoxy into PSU, it was about one time larger than that of PSU into epoxy under each processing temperature, which means the diffusion process was easier than the precipitation process due to the limited mobility of large molar weight and amorphous long-chain PSU.

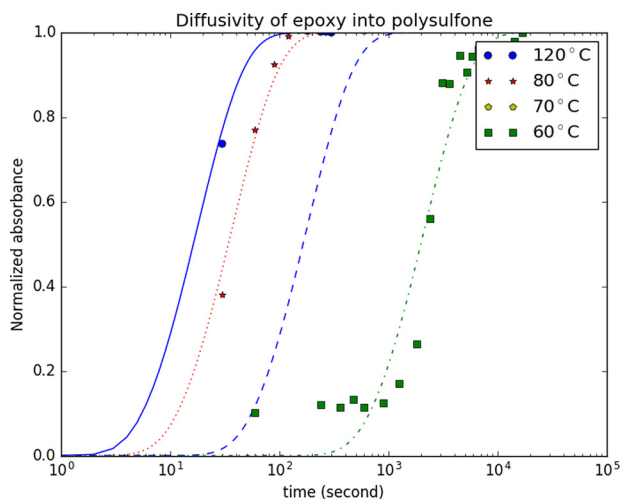


Fig. 6 Diffusivity determination of epoxy into PSU from 60 °C to 120 °C. Normalized absorbance data were obtained from ATR–FTIR experiments. Least square fitting curves were based on Eq. (4) for each condition.

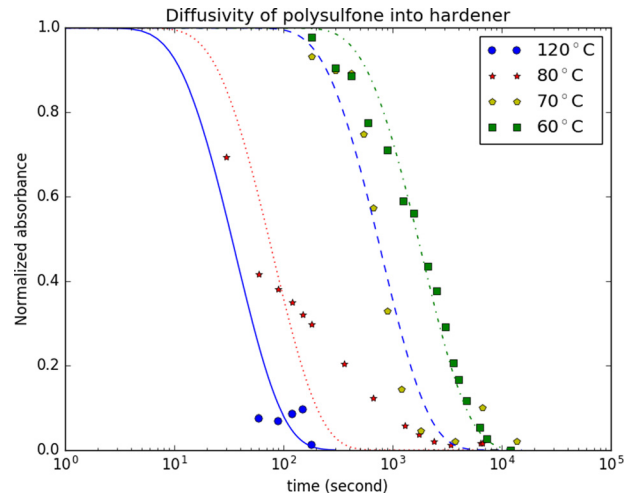


Fig. 7 Diffusivity determination of PSU to hardener from 60 °C to 120 °C. Normalized absorbance data were obtained from ATR–FTIR experiments. Least square fitting curves were based on Eq. (4) for each condition.

Figures 7 and 8 show the experimental results of PSU into hardener and hardener into PSU. The monitored peaks in this case were 2916 cm^{-1} for C–H stretching in the hardener. From 60 °C to 120 °C, the diffusivity of PSU into hardener at each condition was 1.97×10^{-11} , 4.6×10^{-11} , 4.571×10^{-10} , and 1.31×10^{-7} m²/s. The diffusivity of hardener into PSU at each condition was 1.011×10^{-10} , 1.201×10^{-10} , 8.341×10^{-10} , and 1.71×10^{-7} m²/s.

Figure 9 shows the experimental results of 5% PS modified epoxy to PSU. The effect of low-concentration PS additive on the diffusivity of the epoxy into PSU was not significant. For example, the corresponding diffusivities of modified epoxy into PSU were 1.9×10^{-11} m²/s at 60 °C and 1×10^{-10} m²/s at 70 °C. Compared the diffusivity data between the nonmodified and modified epoxy, they were at the same order of magnitude, and the values were close to each other, which indicated that the addition of PS did not influence the diffusivity of the epoxy to the PSU.

Curing Kinetics of Epoxy System. In the ATR–FTIR experiment, the infrared element crystal disk was preheated to the

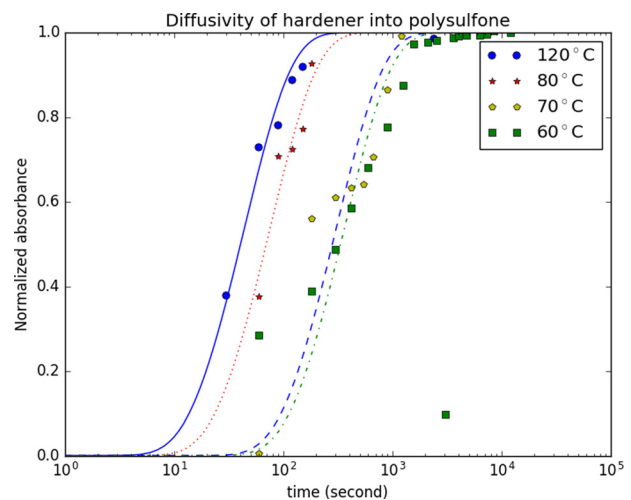


Fig. 8 Diffusivity determination of hardener to PSU from 60 °C to 120 °C. Normalized absorbance data were obtained from ATR–FTIR experiments. Least square fitting curves were based on Eq. (4) for each condition.

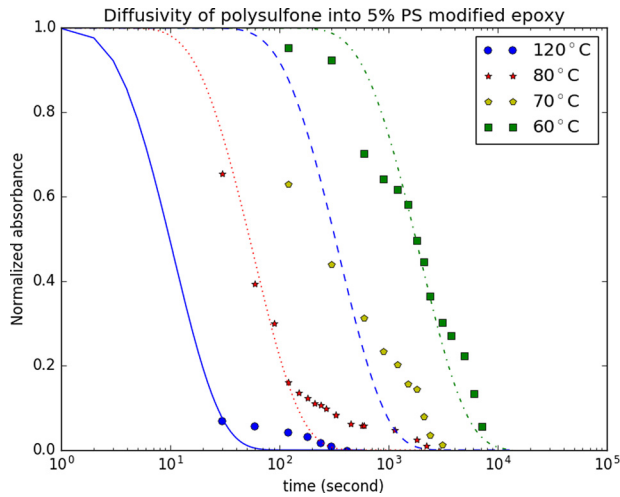


Fig. 9 Diffusivity determination of PSU into 5% PS modified epoxy from 60 °C to 120 °C. Normalized absorbance data were obtained from ATR-FTIR experiments. Least square fitting curves were based on Eq. (4) for each condition.

desired processing temperature. The epoxy was premixed with the hardener, and glass pipet was used to transfer the epoxy onto the crystal surface. The change of the 915 cm^{-1} and 1187 cm^{-1} peaks was monitored during the experiments. The processing temperatures used in the experiments were 80 °C and 120 °C.

Figure 10 shows the curing kinetics of epoxy with and without 5% PS additives cured at 80 °C and 120 °C. The y-axis represents the degree of cure, which is calculated based on the reduction of the uncured epoxy concentration measured in the experiment through monitoring 915 cm^{-1} peak. During the curing process, the epoxide ring opened, branched, and crosslinked with the hardener and other open epoxide rings. Thus, the low molecular weight epoxy began to turn to high molecular weight molecules, which led to gelation and finally turned into solid cured epoxy. The increasing molecular weight and crosslinking epoxy reduced its mobility in the system and changed its solubility. Thus, the curing kinetics played an important role in the diffusion and precipitation process. In order to improve the diffusion and precipitation depth, the curing kinetics must be modified to make the diffusion and precipitation process longer. The low concentration of additive PS has shown the ability to reduce the curing reaction rate of the epoxy system without significantly reducing the glass transition temperature and increasing viscosity of the epoxy, which corresponds to the high crosslinked density and feasibility of resin infusion by vacuum assisted resin transfer molding.

From Fig. 10(a), it shows the curing kinetics of nonmodified epoxy and 5% PS modified epoxy cured at 80 °C. Both trends increase gradually with the increasing curing time. However, the 5% PS modified epoxy showed less degree of cure at the same time compared to the nonmodified epoxy. For example, when time reached 3000 s, the degree of cure of nonmodified epoxy was above 50% but that of 5% PS modified epoxy only reached 35%. The experiment data were a strong evidence that with the PS additives, the curing reaction rate was reduced. This was mainly due to the dilute effect and nonchemical reactive PS to the curing epoxy. From Fig. 10(b), the curing temperature was risen to 120 °C. Based on Eqs. (8) and (9), the reaction coefficient k_1 was 5.308×10^{-6} and k_2 was 0. At the elevated processing temperature, the curing reaction rate increased significantly. Compared to the case under 80 °C, the degree of cure of nonmodified epoxy reached to 40% in 600 s at 120 °C but almost took 2000 s at 80 °C. The degree of cure of 5% PS modified epoxy was also lower than that of the nonmodified case and showed leveling off after 300 s. By using Eqs. (8) and (9), the reaction coefficient k_1 was 1.647×10^{-5} and k_2 was 0.

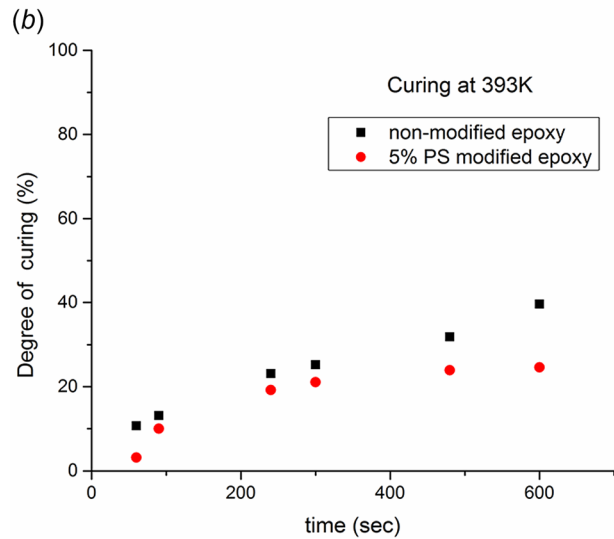
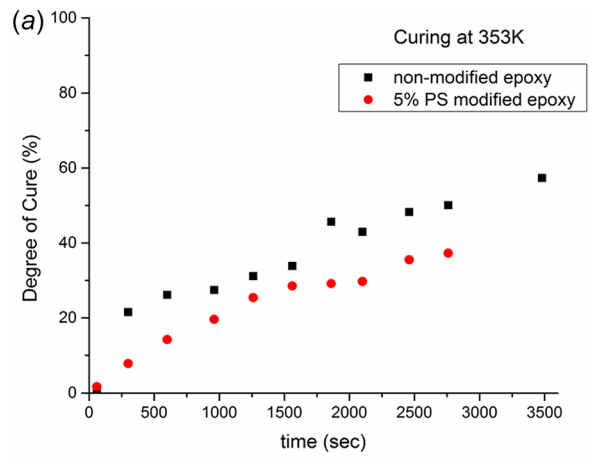


Fig. 10 Degree of curing versus curing time of modified and nonmodified epoxy curing at (a) 80 °C and (b) 120 °C

Diffusion and Precipitation Process Simulation Without Fibers.

The geometry used in the simulation was a rectangular with $320\text{ }\mu\text{m}$ in length and $100\text{ }\mu\text{m}$ in width. At the initial stage, the right half was filled with epoxy and hardener with the concentration ratio of 0.75:0.25, and the left half was filled with PSU with the concentration of 1. The vertical line in the middle is the initial interface between PSU and curing epoxy. The upper and lower boundaries were set as no flux was able to pass through. The left boundary was set as a constant concentration of PSU as 1. The right boundary was set as a constant concentration of epoxy and hardener as 0.75 and 0.25. Since the diffusivities of curing epoxy were higher than that of PSU, the model used corresponding diffusivity for each species. The input diffusivities of the epoxy, hardener, and PSU were obtained experimentally from FTIR, which were also coupled with the curing reaction as shown in Eqs. (13) and (14).

Figure 11 shows the diffusion and precipitation process simulation coupled with curing kinetics of 5% PS modified epoxy curing at 80 °C and 120 °C. The determination of the diffusion depth was to trace the concentration of the epoxy after the interface into the PSU-rich region and reduce to 1% of the initial value. The determination of the precipitation depth was based on tracing the concentration of the PSU into the epoxy-rich region and reducing to 1% of the initial value. Figure 11(a) shows the concentration map of epoxy and PSU across the interface at 80 °C. The diffusion depth was $61\text{ }\mu\text{m}$, and the precipitation depth was

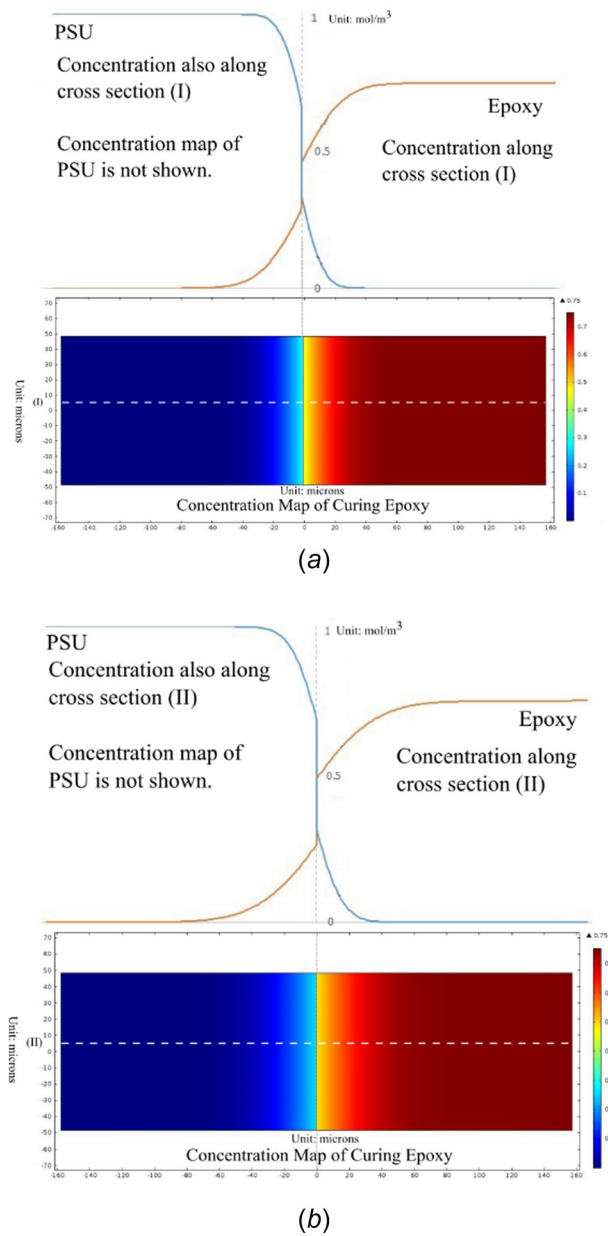


Fig. 11 Diffusion and precipitation process simulation of the 5% PS modified epoxy cured at (a) 80 °C and (b) 120 °C. Concentration map of PSU is not shown. The line plots represent the concentration of epoxy and PSU along dashed line (I).

32 μm . Figure 11(b) shows the concentration map of epoxy and PSU across the interface at 120 °C. The diffusion depth was 109 μm , and the precipitation was 42 μm . From the concentration along dashed lines (I) and (II), there was drop of the concentrations in both cases at the interface. The reason was due to the limited mobility of the swollen TP. For example, the mechanism of PSU precipitating into epoxy-rich region was due to being swollen by the compatible curing epoxy molecules and chain relaxation. The interface was considered as the boundary of the swollen PSU and the generated retractive forces due to the swelling effect made the swollen region still consist of high concentration of the PSU [20]. However, due to the chain relaxation, part of the long chain was able to escape from the swollen region and flow into the epoxy-rich and be quickly distributed in it due to the increased mobility of PSU in the low molecular weight epoxy. As a result, the concentration of PSU had a drop across the interface. The optical observation was shown in Part I of this paper [12]. Figure 12

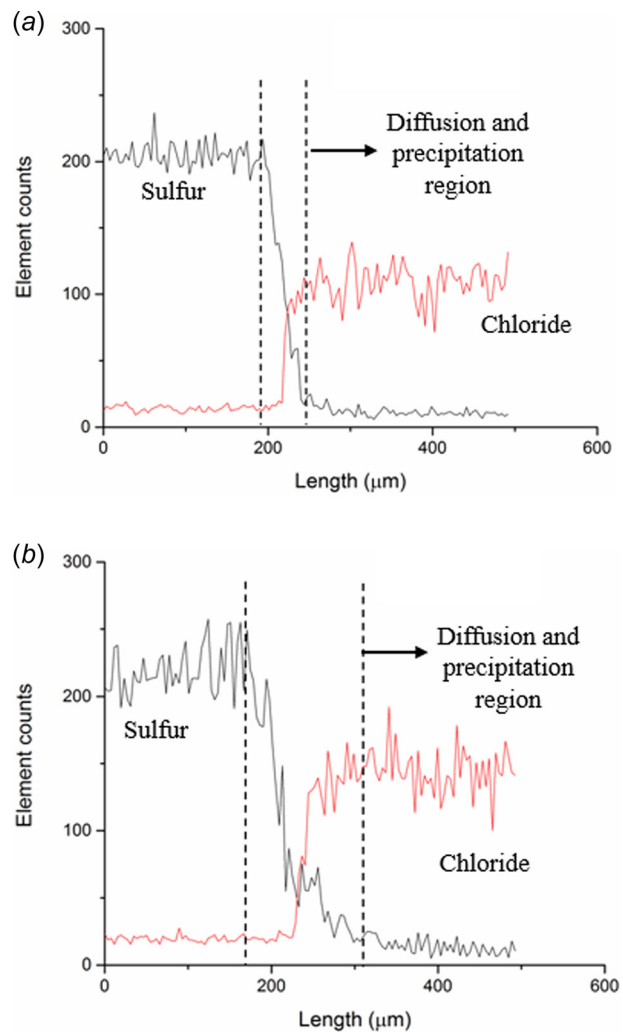


Fig. 12 EDX line scan across the interface of 5% PS modified specimen without fibers cured at (a) 80 °C and (b) 120 °C. The dashed lines represent the width of the diffusion and precipitation region.

shows the EDX line scan across the interface of the specimens modified with 5% PS cured at 80 °C and 120 °C. The sulfur and the chloride were used to represent the PSU and curing epoxy. The dashed lines were used to indicate the diffusion and precipitation region. The line profiles showed the same trends as in the simulation, and the simulated diffusion and precipitation depths were in the same order of magnitude as those measured in the experiments.

Figure 13 shows the diffusion and precipitation depth of the specimen modified with 5% PS obtained from the simulation and experiment. The experimental results were represented by the square and round dots with standard deviation bars on them and indicated that there were no observable diffusion and precipitation if the specimens were cured at room temperatures. When the curing temperature increased to 40 °C and 60 °C, it began to show slight diffusion and precipitation observed from optical microscopy. However, during this temperature range, the difference between diffusion depth and precipitation depth was not significant. The possible reason for this was that the diffusivities of each species at low curing temperature were small, and the mobility of the molecules was limited. Thus, each species were not able to move deep into the other side, and both precipitation depth and diffusion depth were small and close to each other. As the temperatures rose above 80 °C, the diffusion and precipitation region largely increased. The elevated curing temperatures influenced the

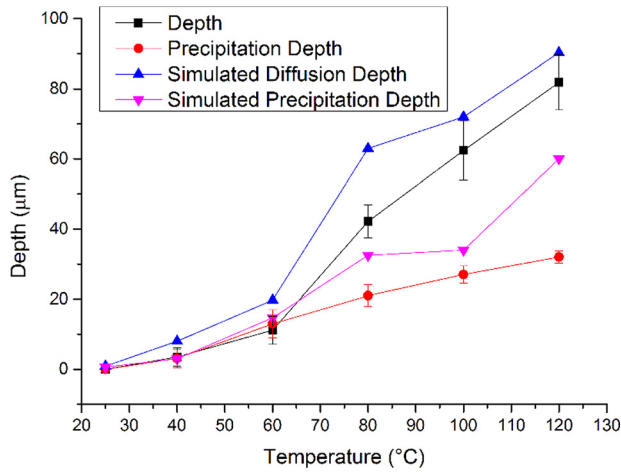


Fig. 13 Diffusion and precipitation depth results from experiments and simulations from 25 °C to 120 °C. The error bars represent standard deviation.

increasing diffusivities of the species and the curing reaction rate. However, the change of curing reaction reaching to the same degree of curing from 80 °C to 120 °C was 1 order of magnitude as can be seen from Fig. 10, and the change of diffusivities of species from 80 °C to 120 °C was several orders of magnitude. This indicated that the high curing temperature influenced more on diffusivity than curing reaction rate, which made the species able to move much larger distances compared to the case under low curing temperatures, especially for the low molar weight curing epoxy. The simulation results showed trends close to the experiment results. The simulated diffusion depths were slightly larger than the diffusion depths observed in the experiment, and the simulated precipitation depths were almost the same as the precipitation depths at the beginning but larger than those at the higher curing temperatures. Both simulated depth curves were at the same order of magnitude as the experimental results. The reason that the simulation results were slightly larger than the experiment results was that the cease of the diffusion and precipitation process was not exactly when the degree of curing reached 0.6, it was some point before 0.6 [13]. Thus, the time window for the

diffusion and precipitation process to carry out was smaller than the time window used in the simulation, which led to the difference between the simulation results and the experiment observations.

Diffusion and Precipitation Process Including Fibers. In this case, the geometry was rectangular with the same size as that in the simulation without considering fibers. However, there were white circles in the epoxy-rich region, which represented the fiber beams. The diameter of the circles was 15 µm, which was the same as the actual size of one fiber beam. The surfaces of the fiber beams were set as impermeable for PSU, epoxy, and hardener in both diffusion and precipitation directions in the simulation.

Figure 14 shows the simulation results of the typical concentration profile of curing epoxy with fiber structures cured at 80 °C. The corresponding concentration map of PSU was not shown here. Line (I) was the line met with the fiber beams at the first column. Line (II) was the line through the center of the geometry, which went through the small gap between the fiber beams at the first column. The line plots of the epoxy and PSU concentration along lines (I) and (II) were superimposed on the top and bottom of the concentration map. In the line plots, concentration of curing epoxy was constant high at the far field away from the interface and reduced to zero after passing through the interface. The corresponding concentration of PSU had the opposite trend compared to the curing epoxy. The gaps between the lines were indicated that these regions were fiber beams, where there was no curing epoxy or PSU. In the center line (II), both PSU and curing epoxy concentrations reduced sharply after the interface, and the concentration drop at the interface was smaller compared to the simulation results without the existence of fibers. In line (I), after the interface, due to existence of the fibers, the slope of the PSU concentration reduced and approved to zero before discontinued. The reason was that the fiber beams acted as obstacles and hedged the flow motion of the curing epoxy and PSU, which was shown in the magnified interface region.

As a comparison, Fig. 15 shows the simulation concentration map of curing epoxy and line plot of curing epoxy and PSU at 120 °C. The corresponding concentration map of PSU was not shown here. The upper and lower line plots represented the concentration changes along line (I) and line (II). Compared to Fig. 14, at high curing temperature, the diffusion depth (the

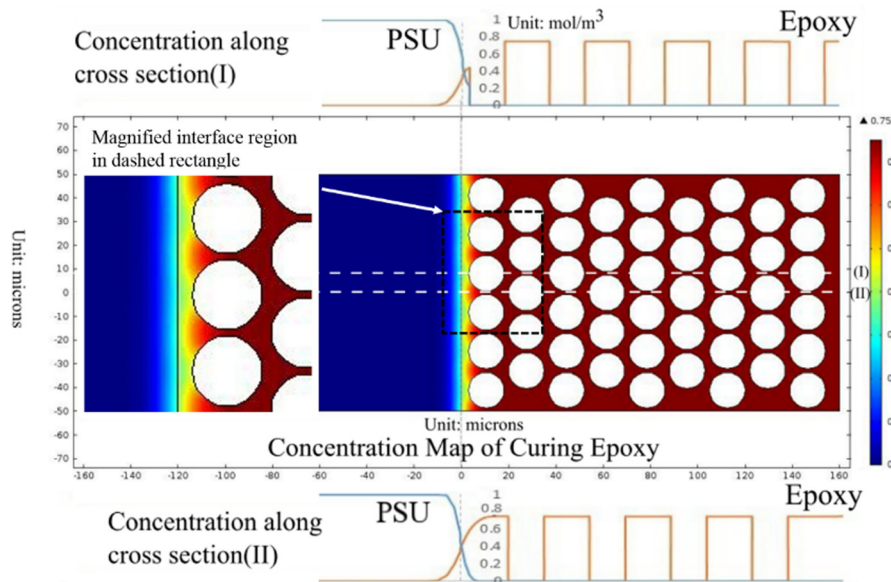


Fig. 14 Diffusion and precipitation simulation of the 5% PS modified epoxy with fibers cured at 80 °C. Concentration map of PSU is not shown. The line plots represent the concentration along line (I) and line (II) in the concentration map.

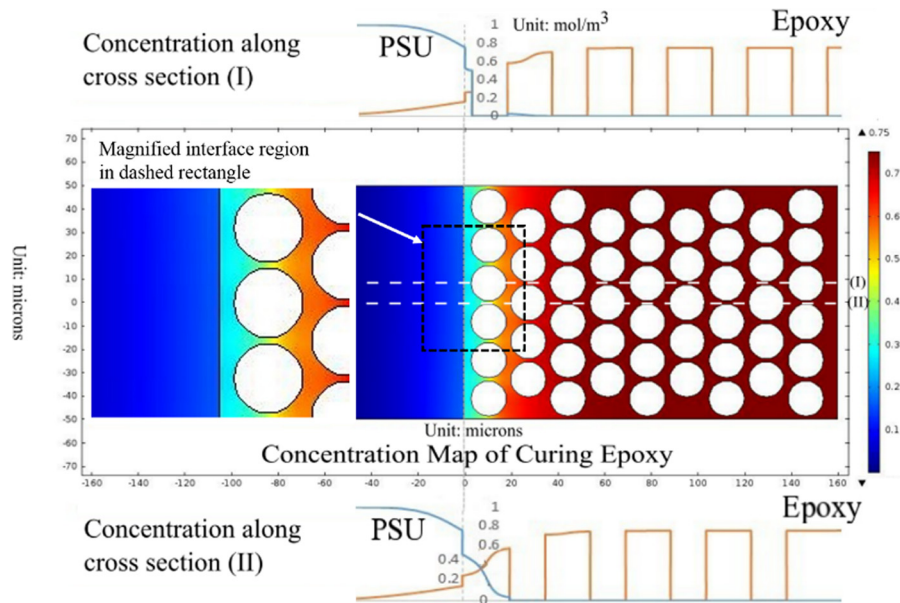


Fig. 15 Diffusion and precipitation simulation of the 5% PS modified epoxy with fibers cured at 120 °C. Concentration map of PSU is not shown. The line plots represent the concentration along line (I) and line (II) in the concentration map.

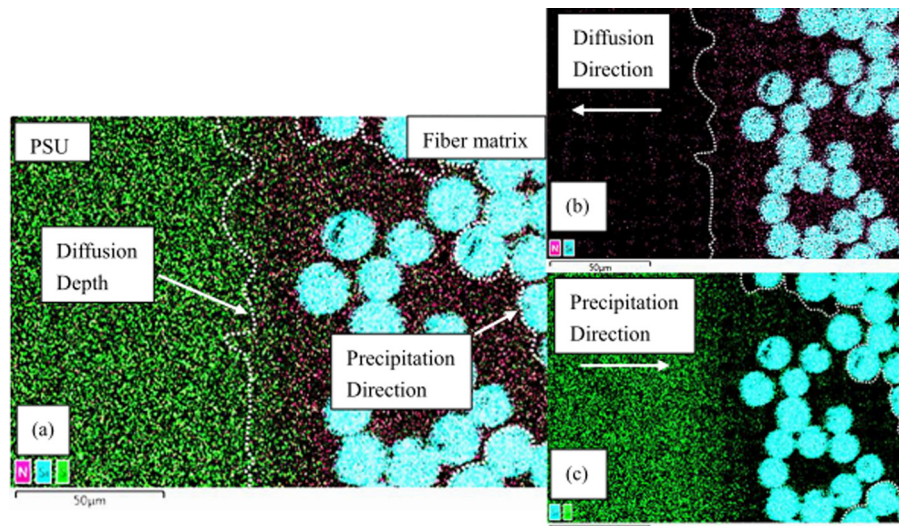


Fig. 16 EDX element mapping of the 5% PS modified specimen cured at 120 °C. Sulfur, nitrogen, and silicon were traced to represent PSU, cured epoxy, and fibers.

distance curing epoxy into PSU-rich region) and the precipitation depth (the distance PSU into epoxy-rich region) were both larger than those at 80 °C. From the center line (II), the concentration changes in the fiber matrix were not uniform: the slope of the curing epoxy was almost flat at the tip of the first contacted fiber beam, increased and reduced again when reached the small gaps between the fibers. The precipitation depth in this case was less than three fiber beam diameters. From line (I), the existence of the fiber beams directly stopped the flow movement of the curing epoxy and PSU before the interface, which represented by the flat curve at the tip of the fiber. After first column of fiber beams, the concentration of PSU was zero, which indicated that the precipitation depth along this line was less than two fiber beam diameters. Both diffusion and precipitation depths were smaller than the case without fiber structures. However, as seen in the magnified interface region, due to the higher curing temperature, there were still significant diffusion and precipitation region.

Figure 16 shows the EDX element mapping of 5% PS modified specimen cured at 120 °C. The element mapping of sulfur, nitrogen, and silicon, which represent PSU, cured epoxy, and fiber beams correspondingly. High density of PSU shows a concentration gradient starting from the middle to the right. The cured epoxy shows the opposite behavior to PSU. The uneven distributed low-concentration PSU in fiber matrix indicated that only part of the PSU separated out from the unstable homogeneous solution during the late stage of the curing process. Other dissolved PSU entangled with the crosslinked epoxy and stayed homogenous as one phase. This evidence matched the optical microscopy observation shown in Part I of this paper [12] that there showed more epoxy diffusing into the PSU-rich region but only a few of PSU precipitates were found in the epoxy-rich region because other PSU did not separate from the solution during the phase separation process. As a comparison, Fig. 17 shows the EDX element mapping of 5% PS modified specimen cured at

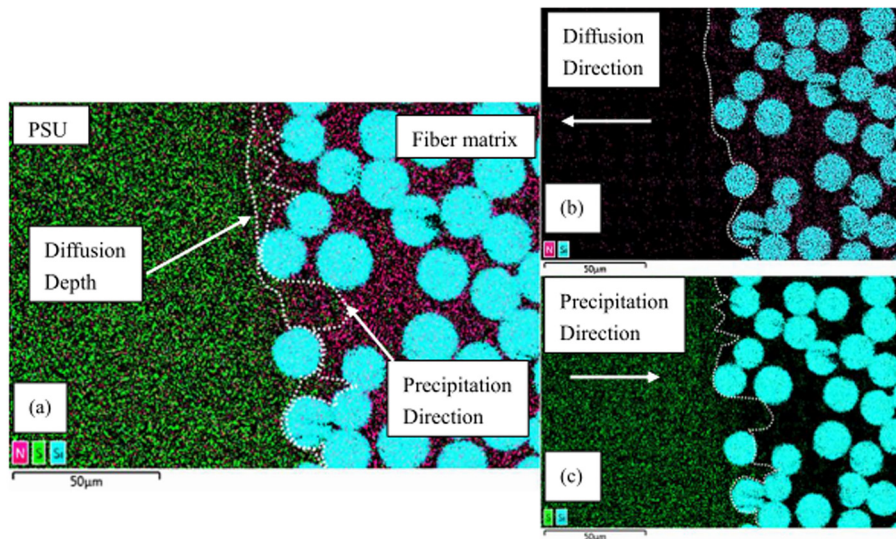


Fig. 17 EDX element mapping of the 5% PS modified specimen cured at 80 °C. Sulfur, nitrogen, and silicon were traced to represent PSU, cured epoxy, and fibers.

80 °C. Due to the low curing temperature, there was a sharp interface, and limited diffusion and precipitation was observed.

Conclusion

The diffusivities of curing epoxy and hardener into PSU were close, and both are higher than the diffusivities of PSU into epoxy or hardener due to the low molecular weight and high mobility of small molecules. Low concentration of PS additive did not influence the diffusivity of the epoxy. However, the PS modified epoxy showed reduced reaction rate compared to the nonmodified epoxy, providing more time for diffusion and precipitation to happen and leading to deep semi-IPN. The diffusivity model coupled with curing kinetics simulation results captured the trends of diffusion and precipitation depths at various curing temperatures. The small gaps between the fiber beams generated large resistance for the TS and TP to pass through and hedged the movement of diffusion and precipitation. From both simulation and experiment results, 5% PS modified specimen cured at 120 °C showed significant diffusion and precipitation region even with the existence of the fiber structures.

Acknowledgment

This research was supported by the National Science Foundation under a GOALI Award No. CMMI-1363328. The authors would also like to thank Ming Gao from Columbia University for providing us ATR-FTIR equipment.

References

- [1] Shetty, R. R., Pavithra, G. K., and Rai, S. K., 2013, "Studies on Mechanical and Fractographic Behavior of Polycarbonate-Toughened Epoxy-Granite Particle Hybrid Composites," *Polym.-Plast. Technol. Eng.*, **52**(11), pp. 1122–1126.
- [2] Pena, G., Eceiza, A., Valea, A., Remiro, P., Oyanguren, P., and Mondragon, I., 2003, "Control of Morphologies and Mechanical Properties of Thermoplastic-Modified Epoxy Matrices by Addition of a Second Thermoplastic," *Polym. Int.*, **52**(9), pp. 1444–1453.
- [3] Xu, Y., Liao, G., Gu, T., Zheng, L., and Jian, X., 2008, "Mechanical and Morphological Properties of Epoxy Resins Modified by Poly(Phthalazinone Ether Sulfone Ketone)," *J. Appl. Polym. Sci.*, **110**(4), pp. 2253–2260.
- [4] Martines, I., Martin, M. D., Eceiza, A., Oyanguren, P., and Mondragon, I., 2000, "Phase Separation in Polysulfone-Modified Epoxy Mixtures. Relationships Between Curing Conditions, Morphology and Ultimate Behavior," *Polymer*, **41**(3), pp. 1027–1035.
- [5] Blanco, I., Cicala, G., and Faro, C. L., 2003, "Improvement of Thermomechanical Properties of a DGEBS/DDS System Blended With a Novel Thermoplastic Copolymer by Realization of a Semi-IPN Network," *J. Appl. Polym. Sci.*, **88**(13), pp. 3021–3025.
- [6] Heitzmann, M. T., Hou, M., Verdt, M., Vandl, L., and Paton, R., 2011, "Morphology of an Interface Between Polyetherimide and Epoxy Prepreg," *Adv. Mater. Res.*, **393–395**, pp. 184–188.
- [7] Milliman, H. W., Boris, D., and Schiraldi, D. A., 2012, "Experimental Determination of Hansen Solubility Parameters for Select POSS and Polymer Compounds as a Guide to POSS—Polymer Interaction Potentials," *Macromolecules*, **45**(4), pp. 1931–1936.
- [8] Yun, N. G., Won, Y. G., and Kim, S. C., 2004, "Toughening of Epoxy Composite by Dispersing Polysulfone Particle to Form Morphology Spectrum," *Polym. Bull.*, **52**(5), pp. 365–372.
- [9] Vandl, L. J., Hou, M., Veidt, M., Truss, R., Heitzmann, M., and Paton, R., 2012, "Interface Diffusion and Morphology of Aerospace Grade Epoxy Co-Cured With Thermoplastic Polymers," 28th International Congress of the Aeronautical Sciences (ICAS), Brisbane, Australia, Sept. 23–28.
- [10] Bulter, C. A., McCullough, R. L., Pitchumani, R., and Gillespie, J. W., 1998, "An Analysis of Mechanisms Governing Fusion Bonding of Thermoplastic Composites," *J. Thermoplast. Compos. Mater.*, **11**, pp. 338–363.
- [11] Sorrentino, A., Gorrasi, G., Tortora, M., and Vittoria, V., 2006, "Barrier Properties of Polymer/Clay Nanocomposites," *Polym. Nanocompos.*, **11**, pp. 273–292.
- [12] Bian, D., Beeksmma, B. R., Shim, D. J., Jones, M., and Yao, Y. L., "Interlaminar Toughening of GFRP, Part 1: Improved Diffusion and Precipitation" (unpublished).
- [13] Sanford, W. M., 1987, "Curing Behavior of Thermosetting Resin Composites," Ph.D. thesis, University of Delaware, Newark, DE.
- [14] Skourlis, T. P., and McCullough, R. L., 1994, "Measurement of Diffusivity of a Liquid Diamine in Solid Epoxies Using Attenuated Total Reflectance Infrared Spectroscopy," *J. Appl. Polym. Sci.*, **52**(9), pp. 1241–1248.
- [15] Rajagopalan, G., Immordino, K. M., Gillespie, J. W., and McKnight, S. H., 2000, "Diffusion and Reaction of Epoxy and Amine in Polysulfone Studied Using Fourier Transfer Infrared Spectroscopy: Experimental Results," *Polymer*, **41**(7), pp. 2591–2602.
- [16] Hardis, R., 2012, "Cure Kinetics Characterization and Monitoring of an Epoxy Resin for Thick Composite Structures," *M.Sc. thesis*, Iowa State University, Ames, IA.
- [17] Dibenedetto, A. T., 1987, "Prediction of the Glass Transition Temperature of Polymers: A Model Based on the Principle of Corresponding States," *J. Polym. Sci.*, **25**(9), pp. 1949–1969.
- [18] Rajagopalan, G., Gillespie, J. W., and McKnight, S. H., 2000, "Diffusion of Reacting Epoxy and Amine Monomers in Polysulfone: A Diffusivity Model," *Polymer*, **41**(21), pp. 7723–7733.
- [19] Rajagopalan, G., Narayanan, C., Gillespie, J. W., and McKnight, S. H., 2000, "Diffusion and Reaction of Epoxy and Amine in Polysulfone—Transport Modeling and Experimental Validation," *Polymer*, **41**, pp. 8532–8556.
- [20] Mangaraj, D., Bhatnagar, S. K., and Rath, S. B., 1963, "Cohesive-Energy-Density of High Polymers. Part III: Estimation of C.E.D by Viscosity Measurement," *Macromol. Chem. Phys.*, **67**(1), pp. 75–83.